Journal of Magnetic Resonance **156,** 113–121 (2002)
doi:10.1006/jmre.2002.2530

Frequency Dependence of EPR Signal Intensity, 250 MHz to 9.1 GHz

George A. Rinard,* Richard W. Quine,* Sandra S. Eaton,† and Gareth R. Eaton†,[1]

*Department of Engineering and †Department of Chemistry and Biochemistry, University of Denver, Denver, Colorado 80208-2436

Received November 19, 2001; revised March 12, 2002; published online May 31, 2002

Experimental EPR signal intensities at 250 MHz, 1.5 GHz, and 9.1 GHz agree within experimental error with predictions from first principles. When both the resonator size and the sample size are scaled with the inverse of RF/microwave frequency, ω, the EPR signal at constant B_1 scales as $\omega^{-1/4}$. Comparisons were made for three different samples in two pairs of loop gap resonators. Each pair was geometrically scaled by a factor of 6. One pair of resonators was scaled from 250 MHz to 1.5 GHz, and the other pair was scaled from 1.5 GHz to 9 GHz. All terms in the comparison were measured directly, and their uncertainties estimated. The theory predicts that the signal at the lower frequency will be larger than the signal at the higher frequency by the ratio 1.57. For 250 MHz to 1.5 GHz, the experimental ratio was 1.52 and for the 1.5-GHz to 9-GHz comparison the ratio was 1.14.

INTRODUCTION

Multifrequency EPR in which the RF/microwave frequency is selected to suit the experiment is increasingly being used to sort out multiple contributions to EPR signals. In addition, better penetration of the body and lower energy deposition makes low radiofrequencies (RF) advantageous for biomedical EPR. Therefore, it is important to be able to predict EPR performance as a function of RF/microwave frequencies (*1–6*).

Derivations from first principles predict that EPR signal intensity will depend on frequency less strongly, by a factor of ω (*7–11*), than stated in the monograph by Poole (*12*). The predictions have been confirmed for comparisons of VHF and L-band pulsed EPR (*13*) and for S-band and X-band pulsed EPR (*10, 11*). Background literature was comprehensively cited in our prior papers and will not be repeated here. In this paper we present experimental confirmation of our predictions for CW EPR, which in some ways is more difficult than pulsed EPR (*9, 10*).

BACKGROUND

Table 1 gives the results of our derivations and shows the frequency dependence of EPR signal intensity for three different cases. The results in Table 1 are based on a lumped-element resonator, e.g., a loop-gap resonator (LGR). Lumped-element resonators allow the most flexibility in selecting resonator size to meet sample requirements and are the only practical resonators for frequencies much below 1 GHz. The predictions in Table 1 are consistent with commonly cited predictions for NMR, when the same assumptions are made.

It has been shown (*7–10*) that the EPR signal voltage, V_s, is given by

$$V_s = \chi''(\omega)\eta Q\sqrt{Z_0 P}, \qquad [1]$$

where $\chi''(\omega)$ is the imaginary component of the effective RF susceptibility, η is the filling factor, Q is the loaded quality factor of the resonator, Z_0 is the characteristic impedance of the transmission line, and P is the RF/microwave power to the resonator.

One of the difficulties in applying this equation to quantitative EPR is estimating the filling factor. In this paper we avoid this problem by scaling the sample size and all resonator dimensions with the inverse of frequency so that the filling factor remains constant in our comparisons.

For convenience, we cite here useful equations from our prior papers, with notation specific to loop-gap resonators (LGR), for Q and B_1,

$$Q = \left(\frac{\sqrt{2}}{8}\sqrt{\mu_0}\sqrt{\sigma}\right) d\omega^{1/2}. \qquad [2]$$

In this equation, d is the diameter of the LGR, μ_0 is the permeability in a vacuum, σ is the conductivity of the surface of the resonator, and ω is the frequency.

$$B_1 = \frac{2^{1/4}\sigma^{1/4}\mu_0^{3/4}\sqrt{P}}{\omega^{1/4}\sqrt{\pi d z}}, \qquad [3]$$

where the length of the LGR is z.

When resonator and sample are scaled with wavelength and B_1 is kept constant, the EPR signal varies as $\omega^{-1/4}$ (*7–11*). This will also be the frequency dependence of S/N when the noise is predominantly thermal noise. Meeting these conditions means that the EPR signal strength will actually increase as frequency is reduced.

[1] To whom correspondence should be addressed. E-mail: geaton@du.edu.

1090-7807/02 $35.00

TABLE 1
Frequency Dependency of EPR Parameters

	Case 1 Constant sample size Constant LGR size	Case 2 Sample size $\propto 1/\omega_0$ LGR size $\propto 1/\omega_0$	Case 3 Constant sample size LGR size $\propto 1/\omega_0$
L	1	ω_0^{-1}	ω_0^{-1}
R	$\omega_0^{1/2}$	$\omega_0^{1/2}$	$\omega_0^{1/2}$
Q	$\omega_0^{1/2}$	$\omega_0^{-1/2}$	$\omega_0^{-1/2}$
η	1	1	ω_0^{3}
EPR signal, constant P	$\omega_0^{3/2}$	$\omega_0^{1/2}$	$\omega_0^{7/2}$
$B_1/\sqrt{P}$	$\omega_0^{-1/4}$	$\omega_0^{3/4}$	$\omega_0^{3/4}$
P for constant B_1	$\omega_0^{1/2}$	$\omega_0^{-3/2}$	$\omega_0^{-3/2}$
EPR signal-constant B_1	$\omega_0^{7/4}$	$\omega_0^{-1/4}$	$\omega_0^{11/4}$

Note. L, R, Q, and η are the inductance, resistance, quality factor, and filling factor of the resonator; P is RF power; and B_1 is the RF magnetic field intensity.

These conditions are often easily met for relatively small reductions in frequency and even for large reductions in frequency if the sample is unlimited in size. Sample size may be limited if it is, for example, an organ of a live animal. It may not be as limited if it is an extracted biological sample, but practical considerations may limit the available quantity of such samples. Therefore, while the EPR signal may not actually increase with a decrease in frequency, by designing the resonator size and frequency for each application considerable improvement in signal strength is possible, relative to what has commonly been assumed. The above analysis does not include the reduced RF energy deposition and higher RF penetration of biological samples at low frequency. The increased penetration at lower frequencies improves the relative signal strength as the frequency is reduced.

EXPERIMENTAL

A series of experiments was performed to verify the theoretical variation of EPR signal strength with frequency. In (*10, 11*) we showed that extreme care is needed to obtain valid comparisons of the performance of EPR spectrometers, in agreement with the oft-quoted statement of Hyde that "of all the measurements one can make with EPR equipment, the determination of absolute spin concentration is the most difficult" (*14*). These experiments were made methodically, by fully characterizing the resonators, spectrometers, and samples. Corrections were made for the small differences that were unavoidable—the slight change of frequency and Q with sample, for example.

Description of resonators. It was desired to make measurements over a nominal frequency range of 250 MHz to 9 GHz (1 : 36) with the resonator sizes scaled with the inverse of frequency ($1/\omega_0$), case 2 of Table 1. It was not feasible to accomplish this in a single step in our lab. Either the 9-GHz resonator would be impractically small or the 250-MHz resonator would be too large for our magnet. Consequently, the comparison was made in two steps with nominal factors of 6 each, using reentrant loop-gap resonators (LGR) analogous to the one described in (*15*). Four LGR were constructed for VHF, L-band, and X-band. Two of the LGRs were geometrically similar and scaled in size for VHF and L-band. The other two were of a different geometry, but were also geometrically similar and scaled in size for L-band and X-band.

Figures 1 and 2 show the design of the resonators and the physical parameters are given in Table 2. The EPR signals for the VHF and the small L-band resonators formed one comparison, and the

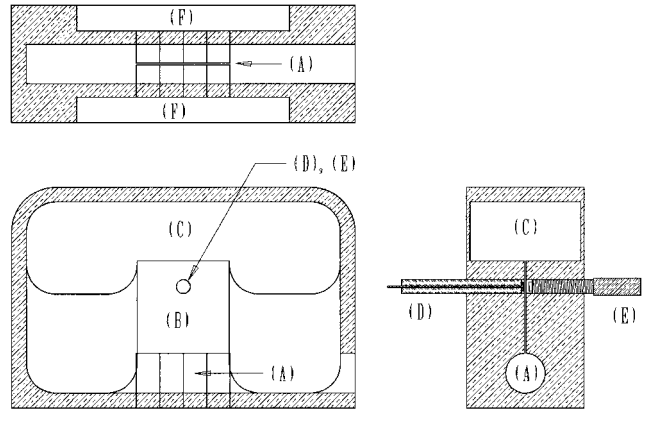

FIG. 1. Three cross-sectional views of the geometry of the VHF and small L-band reentrant LGRs, through the centerline of the sample tube. Dimensions are given in Table 2. Each resonator was machined in two pieces from solid tellurium-copper alloy and fastened together with brass machine screws. The sample is inserted into the cylindrical region (A), which is the loop of the resonator. (B) The resonator gap. The five vertical lines in this region of the loop are slots to allow penetration of the magnetic field modulation. The RF/microwave field is fully contained within the resonator by the reentrant loop (C). The resonator is fed through coax (D) and is tuned by the coupling screw (E). (F) A recessed region that reduces the thickness of the resonator walls and provides room for the field modulation coils.

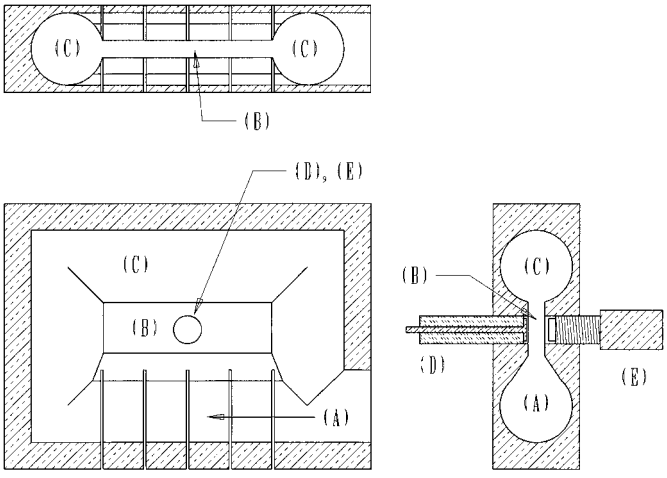

FIG. 2. Three cross-sectional views of the geometry of the large L-band and X-band reentrant LGRs, through the centerline of the sample tube. Dimensions are given in Table 2. (A), (B), and (C) The sample loop, gap, and reentrant loop, respectively. (D) and (E) The feed coax and coupling screw, respectively. Unlike the resonators shown by Fig. 1, all loops of these resonators are the same size. The gap near the sample loop is beveled to reduce the electric field in the vicinity of the sample tube. This helped minimize the change in resonate frequency with sample insertion. The sample holder held the sample tube as far away from the gap as possible for the same reason.

signals from the large L-band and the X-band resonators formed the other. Resonators in each pairing were geometrically similar, so that the B_1 distributions, and thus filling factors, would be geometrically similar and thus directly comparable. In order to keep the RF/microwave aspects as similar as possible, the sample tube wall thickness as well as the slots and spacing between the slots cut in the resonator to facilitate modulation penetration were also scaled by a factor of 6. The design of these resonators is implicit in the equations in Ref. (*16*), which also provides equations describing the series capacitance coupling that was utilized. We did not put a protective noble metal plating on these resonators because the plating could have changed the skin effect resistance and affected the variation of Q with frequency.

Sample preparation. To facilitate the intercomparisons with a minimum number of variables, it was desired to have samples that would have minimal impact on resonator Q. In addition, it was desired to have a variety of samples. Three types of sample were selected for the comparisons: nitroxyl radical in fluid solution (4-oxo-2,2,6,6-tetramethyl-1-piperidinyloxy, Tempone, also called 4-oxo-TEMPO, Aldrich Chemical Co.); the solid organic radical α,γ-bisdiphenylene-β-phenylallyl 1 : 1 complex with benzene (BDPA, Aldrich Chemical Co.); and a sulfur radical in the mineral ultramarine blue (Pfaltz & Bauer).

Tempone was dissolved in 4 : 1 mineral oil (Aldrich 16140-3) : toluene to yield a 0.23-mM solution. This solution had sufficient viscosity to inhibit line broadening due to collisions with O_2 but still sufficient mobility that all three nitrogen hyperfine lines were of the same intensity. To avoid possible differences in O_2 concentrations, samples were not degassed.

BDPA powder (2.18 mg) was mixed with 50 g finely ground KCl. Ultramarine blue (0.5 g) was mixed with 50 g of finely ground KCl. The BDPA and ultramarine blue were not ground to avoid changing the samples. Weighed aliquants of the KCl mixtures were added to quartz tubes and tapped on a resilient surface until settling was complete. The weight of sample per unit volume was used in the calculations comparing signal intensities. Packing density was slightly lower in the 4-mm o.d. tubes than in the 25-mm o.d. tubes.

The sample tube dimensions were intended to scale with the factor of 6 differences in RF frequency. A small correction was needed, because the 4-mm o.d. quartz tubes had an internal diameter of about 3.15 mm, as determined by volumetric and gravimetric methods. The "one-inch" quartz tubes were about 25.1 mm o.d. and 19 mm i.d. The wall thickness was scaled with the factor of 6 differences in RF frequency in order to maintain constancy of filling factor and of lens effect of the quartz on the RF and microwaves.

Samples were made long enough relative to the region of significant magnetic field modulation so that the positioning of the sample was not critical.

Measurements. The spectrometer has gain, G, and other characteristics that affect the recorded signal. In order to verify the relationships in Table 1, using different spectrometers, each signal must be normalized by dividing out the factors characteristic of the recording spectrometer. Measurements on our EPR spectrometer are conventionally made using field modulation. Field modulation produces the derivative of the spectra. Table 1 describes how the EPR signal varies with frequency, provided that the linewidth does not change and that resonator parameters are not changed with sample.

Equation [4] was used to normalize the EPR spectrum height for sample and spectrometer characteristics,

$$|SH_{Norm}| = \frac{K \times DH \times \Delta B^2}{B_m \times G \times n_s}, \qquad [4]$$

where

SH_{Norm} = normalized height of the spectrum
K depends on lineshape but is not a function of frequency
DH = peak-to-peak amplitude of the measured derivative spectrum
ΔB = peak-to-peak linewidth of the first derivative signal (Gauss)

TABLE 2
Physical Parameters of LGRs

Dimensions in mm	VHF	Small L-band	Large L-band	X-band
Loop diameter	25.8	4.3	25.8	4.3
Loop length	60	10	60	10
Gap width	60	10	24	4
Gap thickness	0.406	0.068	6.1	1.02

B_m = peak-to-peak amplitude of the modulation (Gauss)
G = total gain of the spectrometer
n_s = number of scans.

This equation gives the normalized value of the peak-to-peak height of the spectrum per gauss of modulation amplitude per scan. Division by n_s is required since successive scans are added, not averaged, in the software used.

Measurement of resonator efficiency, Λ. If all the spectra at different frequencies are taken at values of incident power that produce the same B_1 in the resonator and measurement conditions are ideal, signals corrected using Eq. [4] can be used to verify the predictions in Table 1. However, making measurements at the same B_1 requires knowing the resonator efficiency, $\Lambda = B_1/\sqrt{Watt}$, *a priori*, for each resonator. Table 1 can be used to predict what the ratio of this power should be. However, this prediction needs to be verified; also the power required for a given B_1 is dependent on the change of Q with sample. Because of this interrelationship, measurements were made on samples at powers well below saturation, and postprocessing was used to find the signal ratios for constant B_1. This is a valid approach since the signal amplitude for a nonsaturated sample is proportional to B_1 (or $\sqrt{P}$, as shown by Eq. [1]).

To provide a basis for making the corrections described above and to verify the Λ predictions in Table 3, measurements of Λ were made using the three-pulse null electron spin echo (ESE) method (*17*) and CW saturation. The measured ratios of Λ are 0.25 and 0.27 (low frequency/high frequency), which agree well with that predicted by theory, 0.26. The BDPA spectra are exchange-narrowed (*18*) and have CW absorption lines that are close to Lorentzian in the center, but more nearly Gaussian in the wings. We observed a slight increase in linewidth at lower frequencies for BDPA. The narrowing at higher frequency means that the relaxation time is shorter at lower frequency (*19*), so the B_1 required to achieve the same degree of saturation of BDPA is larger at 250 MHz than at X-band. This argument predicts that CW power saturation of BDPA will estimate a smaller B_1 than will spin echo methods at lower frequency. This trend is what we observe for VHF vs L-band. Since saturation measurements of Λ are relaxation time dependent and since the relaxation time is frequency dependent, we place more confidence in the ESE measurements. These measurements verify the calculated ratio of values of Λ, 0.26, and this was the value used in normalizing the measured values of spectrum height.

TABLE 3
Calculated and Measured Values of Λ ($Gauss/\sqrt{Watt}$)

	Calculated	Ratio low/high[a]	Measured (ESE)	Ratio low/high[b]	% Difference meas. to calc.
VHF	0.96	0.26	0.96[c]	0.25	0
Small L-band	3.7		3.9		5.4
Large L-band	0.47	0.26	0.53	0.27	12.8
X-band	1.8		2.0		11.1

[a] Ratio of Λ at lower frequency to Λ at higher frequency for calculated values.
[b] Ratio of Λ at lower frequency to Λ at higher frequency for measured values.
[c] By CW power saturation.

TABLE 4
Calculated and Measured Values of Resonator Parameters

	ν_0 GHz measured	Q		C pF calculated	L nH calculated
		Measured	Calculated		
VHF	0.25095	1024[a]	1035	56.1	7
Small L-band	1.536	460[b]	423	9.4	1.2
Large L-band	1.624	2866[b]	2917	2.5	4.1
X-band	9.6075	1177[a]	1205	0.41	0.69

[a] Decrement or ring-down method (*20*), on test bench, not on spectrometer.
[b] HP 8753D Network Analyzer.

Measurement of resonator Q. The comparison of measured EPR signals also involves determination of the Q of each resonator. The value of the loaded Q was calculated for each resonator from fundamental considerations. The loaded Q of each empty resonator was then measured to verify theory. The results are given in Table 4, together with calculated estimates for resonator capacitance and inductance. The measurements of Q were repeated many times. Resonator Q was measured by ring down (decrement method (*20*)) following a pulse or by measuring the 3-dB bandwidth, $\Delta\omega$, on an HP 8410 Network Analyzer with 8414A Polar Display and calculating $Q = \omega/\Delta\omega$. The calculations of Q, and hence of B_1, use the resistivity of the metal. For pure copper the resistivity is 1.72×10^8 Ω-m (skin depth of 1.48 μm at 2 GHz) (*21*, p. 636).

The measured values of loaded Q compare well with the calculated values. The value of loaded Q varies with the spectrometer and with sample. The variation of Q with spectrometer is due to the fact that the circulator, which is part of the tuning circuit, does not have perfect isolation. Therefore, at critical coupling on the spectrometer, the resonator itself has a small reflection (typically -20 dB) that balances the circulator isolation at the output of the circulator. The resonator will be somewhat under- or overcoupled depending on the length of the line from the spectrometer to the resonator. The resonator, line, and circulator all are part of the tuning circuit, and the loaded resonator Q can vary as much as $\pm 20\%$. Because of this, the loaded Q was measured on the spectrometer with and without sample, and these values were used in postprocessing. Table 4 also gives the measured resonant frequencies of the as-built resonators without sample. The actual operating Q's with sample were used in the final comparison of signal height.

Small corrections for measurement conditions. All signals were compared as the ratio of SH_L/SH_H, where SH_L is the normalized height at the lower frequency and SH_H is that for the higher frequency. According to Table 1, the normalized signal

height for a frequency ratio of 1 : 6 is

$$\frac{SH_L}{SH_H} = \left(\frac{1}{6}\right)^{-\frac{1}{4}} = 1.57. \qquad [5]$$

The multiplying factor to correct the normalized signal height ratio to the same B_1 is

$$F_P = \sqrt{\frac{P_H}{P_L}} \times 6^{\frac{3}{4}} \times \left(\frac{q_H}{q_L}\right)^{\frac{1}{2}}, \qquad [6]$$

where the first term involves the ratio of the powers used for each sample at their respective frequencies; the second term normalizes the signal height ratio to the same B_1 as prescribed by Table 1 and verified by Table 3; and the third term involves $q = Q_{Sample}/Q_{Empty}$ which is the ratio of the loaded Q of the resonator with a sample to that when it is empty. The last term is required to account for the effective change in resonator resistance, R, due to sample loss in addition to that due to frequency, which is predicted in Table 1.

The remaining correction factors account for experimental tolerances in sample size and density, and frequency and Q changes with sample are predicted by

$$F_{\chi_0} = \frac{PackingDensity_H}{PackingDensity_L}, \qquad F_{\varpi} = \frac{freq_H}{freq_L} \times \frac{1}{6},$$
$$F_{\eta} = \left(\frac{dia_H}{dia_L}\right)^2 \times 6^2, \qquad F_Q = \frac{Q_H}{Q_L} \times 6^{\frac{1}{2}}. \qquad [7]$$

F_{χ_0} is a small factor to account for the difference in packing in the large and small tubes. F_{ω} accounts for the small change in frequency caused by the sample. F_{η} accounts for the small change in filling factor due to the tolerance on tube size. The filling factor is proportional to the volume of the sample, which ideally is proportional to ω^{-3}. Since the length of the sample is determined by the geometry of the resonator, it is already proportional to ω^{-1} so this term involves the ratio of the diameter of the sample tubes squared. If the ratio of low-frequency to high-frequency sample tubes is 6, this factor is one. F_Q accounts for the change in Q with sample, which is inherent in Eq. [1]. This is in addition to the effect on Λ, which is accounted for in Eq. [6]. According to Table 1, Q varies as $\omega_0^{-1/2}$; therefore, if Q has the predicted ratio of $6^{-1/2}$, F_Q in Eq. [7] will be one. If it is not exactly this ratio, than F_Q will vary directly with Q as predicted by Eq. [1]. In our results all of these factors are small, the largest typically being F_Q.

Spectrometers. Three spectrometers were used to compare EPR signals at three frequencies, stepped by factors of 6, 250 MHz, 1.5 GHz, and 9 GHz. The bridges in all three spectrometers are based on circulators. The L-band spectrometer is described in (*15*); the X-band spectrometer was a commercial Varian E-9 upgraded to an E109 equivalent. The X-band spectrometer uses diode detection, and the 250-MHz and L-band spectrometers use DBM detection. All three spectrometers follow the RF/microwave phase-sensitive detection with phase-sensitive detection at the magnetic field modulation frequency. The 250-MHz spectrometer, described in (*22*), includes a 4-coil, air-core electromagnet, a reflection LGR, and a reference arm bridge. The RF frequency source was a Fluke 6080A. The amplifiers after the double-balanced mixer (DBM) were the same as in the L-band spectrometer (*15*) at the time of these measurements. The output of the bridge goes to a Stanford Research SR844 lock-in amplifier, whose reference is the modulation frequency. Although there is a digital output from the SR844, we used the analog output, analogous to the analog output from the Varian E-Line consoles used at L-band and X-band, so that the digitization steps and data acquisition and analysis software were the same for all of the spectrometers.

Measurement of spectrometer gains. In order to compare EPR signal amplitudes for two spectrometers, it is necessary to know the actual gain of the signal from the resonator to the final recorded signal. The transfer function of the bridge, the console, and the digitizing system must all be known. We measured the end-to-end gain of the spectrometer, normalized to a console gain setting on the spectrometer of unity. In this way, the gain for a specific experiment is the end-to-end gain multiplied by the console gain setting. The end-to-end gain was measured using two methods. The first method was to input a known amplitude modulated source and measure the output. The second method was based on measuring the output noise with and without a calibrated noise source on the input. The gains measured in both cases were comparable, but the noise source method gave the most reliable and most reproducible results. This noise source method is very easy to use and depends only on the calibration of the noise source and an accurate measurement of the noise effective bandwidth. It also provides the noise figure (NF) of the spectrometer, based on thermal noise and system losses. This is the method that was used in the comparison and is described below.

The available noise power output from a two-port network is

$$P_0 = G_P k_B T B + P_E, \qquad [8]$$

where

G_P is the power gain of the network
k_B = Boltzmann's constant = 1.3805×10^{-23} Joule/K
T = temperature of input thermal noise source (K)
B = bandwidth (Hertz)
P_E = noise power added by the network.

It is convenient to define an equivalent noise temperature of the network as

$$T_E = \frac{P_E}{G_P k_B B}. \qquad [9]$$

T_E is not the actual temperature of the network but is the effective

increase in the noise temperature of the input noise source that would produce the same output noise power if the network itself were noiseless. This allows all sources of noise in the network to be treated as an equivalent noise temperature whether it is thermal noise or from some other source. With this definition it is possible to rewrite Eq. [8] as

$$P_0 = G_P k_B (T + T_E) B. \quad [10]$$

For gain and noise figure measurements using a calibrated noise source, let T_0 be the temperature of the input noise source when the noise source is off and T_{NS} be the equivalent temperature of the noise source when the noise source is on. Taking the ratio of Eq. [10] for $T = T_{NS}$ and $T = T_0$ respectively gives

$$y = \frac{P_{ON}}{P_{OFF}} = \frac{V_{ON}^2}{V_{OFF}^2} = \frac{(T_{NS} + T_E)}{(T_0 + T_E)}, \quad [11]$$

where

$P_{ON}(V_{ON})$ = output power (RMS voltage) with noise source on
$P_{OFF}(V_{OFF})$ = output power (RMS voltage) with noise source off.

Equation [11] can be solved for T_E

$$T_E = \frac{(T_{NS} - yT_0)}{(y - 1)}. \quad [12]$$

Equation [10] with $T = T_{NS}$ can be solved for the gain

$$G = \sqrt{\frac{V_{ON}^2}{kBZ_0(T_{NS} + T_E)}}, \quad [13]$$

where $G = \sqrt{G_P}$ = voltage gain and Z_0 = Characteristic impedance at the measuring point.

Equation [12] gives the effective noise temperature of the spectrometer and Eq. [13] gives the voltage gain. Equation [12] can be substituted into Eq. [13] giving an expression for the voltage gain in terms of measured quantities,

$$G = \sqrt{\frac{(V_{ON}^2 - V_{OFF}^2)}{k_B B Z_0 (T_{NS} + T_0)}}. \quad [14]$$

The noise figure of the network (spectrometer) is defined as the ratio of the total noise power output when the input noise source is at standard temperature (290 K) to what the noise power output would have been if the network were noiseless. This can be written as

$$NF = \frac{P_0}{G_P k_B T_0 B}. \quad [15]$$

Alternatively, we can take the ratio of Eq. [10] with $T = T_0$ to Eq. [10] with $T = T_0$ and $T_E = 0$:

$$NF = 1 + \frac{T_E}{T_0}. \quad [16]$$

The noise figure is a ratio of powers and is often written in dB:

$$nf = 10 \log(NF). \quad [17]$$

The voltage gain, G, and noise figure, nf, for each spectrometer is given in Table 5.

TABLE 5
Measured Voltage Gain and Noise Figure for the Spectrometers

System configuration	Preamp	End-to-end voltage gain	Noise figure, nf dB
X-band E-9	None	2.306×10^3	11.2
X-band E-9	Low gain	2.123×10^4	2.8
L-band, 1.536 GHz	None	566	19.3
L-band, 1.536 GHz	Low gain	1.234×10^4	2
L-band, 1.536 GHz	High gain	4.711×10^4	1.9
VHF, 256 MHz	None	147	10.8
VHF, 256 MHz	Low gain	776	4
VHF, 256 MHz	High gain	3865	3.3

Measurement of modulation amplitude. Magnetic field modulation was achieved with coils wound to fit the geometry of each resonator and magnet. For the 250-MHz LGR the coils were modulated at 45.3 KHz, since the large, about 180-mm diameter, coils exhibited some self-resonance near 100-KHz. The L-band and X-band spectra used 100-KHz modulation driven by modules in Varian E-line consoles.

The EPR signal intensity is linear with magnetic field modulation amplitude for all values of the modulation as long as the modulation is less than about half of the linewidth (*12*). A sample of BDPA and the data in Table 10-1 of (*12*) were used to calibrate the modulation amplitude on the Varian E-9 with a TE_{102} cavity. This calibration was then used to verify the calibration of the voltage output of a search coil. The search coil was about 2 mm in diameter and consisted of about 50 turns of size 40 wire. The coil was mounted at the inside bottom of a 4-mm o.d. EPR tube with its axis normal to the tube's axis. The coil output was 0.225 mV per kHz per gauss. This coil was then used to measure the modulation amplitude inside the 1.5-GHz and 250-MHz resonators. The uncertainty in these measurements is estimated to be about 5%, due largely to the linewidth of the BDPA sample used in the calibration.

The search coil was used to measure the modulation amplitude at various positions in the resonators. In the small resonators, the coil was as large as the spacings between the slots, but the slot spacings were scaled by a factor of six in the large resonators, so the measured modulation amplitude appeared more constant along the length of the resonator in the small resonators than in the large resonators. The combined distribution of modulation

and B_1 was measured along the axis of the sample region by using a small sample of BDPA in the large L-band LGR and in the X-band LGR. The response curves for these two resonators, which were designed to scale by a factor of 6, could be superimposed. It was found that the modulation amplitude was at least as uniform as the B_1.

Dielectric properties of the samples. Inherent in the comparisons is the assumption that the dielectric properties of the samples are the same at the three frequencies. Some data in support of this assumption are provided in Alger (*22*, p. 153), and by the Q and frequency changes observed when samples were placed in the 4 resonators tested.

The density of pure KCl is 1.98 g cm^{-3}. The density of the BDPA and ultramarine blue samples mixed with ground KCl were 1.18 to 1.27 g cm^{-3}. The dielectric constant of KCl is probably similar to that of KBr, $\varepsilon'/\varepsilon_o = 4.9$, $\tan\delta = 2$ to 2.3×10^{-4} (data at 10^6 and 10^{10} Hz). The values for fused quartz are $\varepsilon'/\varepsilon_o = 3.78$, $\tan\delta = 1 \times 10^{-4}$ at 10^6 Hz, 0.6×10^{-4} at 3×10^9 Hz, and 1×10^{-4} at 10^{10} Hz (*22*, p. 153; *23*).

The scaling arguments assume that the effect of, for example, 3-mm quartz at 1.5 GHz is the same as that of 0.5-mm quartz at 9 GHz (principle of similitude).

Error analysis. An error analysis was made based on Eq. [1] taking into consideration the accuracy with which the factors in Eq. [1] can be determined and also on our ability to control the experimental parameters so that a comparison of the results is valid. Some of the experimental parameters, B_1 for example, are not explicit in Eq. [1]. Spectrometer gain and modulation amplitude do not appear in Eq. [1], but occur to the first power in the output signal. The susceptibility, χ'', is directly proportional to frequency, and the error in frequency was considered to be negligible. The filling factor, η, was the same within constructional tolerances for each of the two pairs of LGR. Experimental variations in filling factor include sample-packing density to the first power and the tube diameter squared. In addition the signal amplitude is proportional to the spectral width to the -2 power. For error analysis, the square root of power in Eq. [1] includes all the estimated uncertainties in setting the power and errors in Λ since the experiment depends on B_1 being constant.

Some parameters were easily controlled and contribute errors of only a few percent. Samples were prepared gravimetrically and volumetrically and are judged to be within 1% in spin concentration. Sample tube diameters are least certain for the nominal 4-mm o.d. tubes, whose i.d. is estimated to be 3.1 ± 0.05 mm. This contributes about 1.7% uncertainty to the comparison of 4-mm and 25-mm tubes. Variations in sample temperature due to room temperature variations and due to resonator temperature variations are judged to contribute less than 1% uncertainty. The noise source used to measure spectrometer gain was certified by the manufacturer at frequencies different from those used, but the variation with frequency suggests that we know the noise output to within 0.1 dB (about 2%). The main error in gain measurement was considered to be in determining the noise bandwidth of the spectrometer. The spectrometer gain measurements are estimated to be good to within about 15%. The modulation amplitude, measured as described above, is estimated to be uncertain to about 5%.

The largest uncertainty is in the estimate of B_1 at the sample. As noted above, the power saturation curves can be used to estimate relative B_1 values within about 10%. These values are referenced to the X-band Varian TE_{102} cavity, for which the theoretical values are well established. "Point" samples were used, so the distribution of B_1 over the resonator could be ignored, and the derived values are for B_1 at the center of the resonator. The power required to maximize the 2-pulse $\pi/2$-π echo in the small L-band and X-band LGRs was able to be set to within about 1–2 dB. The power required to null the 3-pulse echo can be estimated to within about 0.2 dB. Note that 0.2 dB is 5% in B_1, 1 dB is 12%, and 2 dB is 26%. The pulse lengths are good to 1% for pulses longer than 100 ns, but a 15-ns pulse may be in error by 10%. Since the CW spectra were obtained in the linear response region, B_1 has a linear impact on the signal intensity. A third estimate of B_1 values is available from first principles using the dimensions of the resonators. To account for these errors, an error bound of 20% was placed on the square root of power in Eq. [1].

The same principles used to estimate the B_1 ratios were used to estimate the resonator Q values. The calculated and measured Q values agree within experimental error, except for the 4.3-mm diameter L-band resonator. It should be noted that the measurement of Q for a resonator that is part of a spectrometer is actually a measurement of the Q of a circuit that includes the circulator (or other directional device), the resonator, the impedance matching device, and the coaxial cables and/or waveguide connecting these items. When one tunes a resonator in a spectrometer to critical coupling, the resonator, itself, is not actually critically coupled. The resonator actually reflects a voltage of magnitude and phase that cancels out the leakage through the circulator. Since the isolation of a circulator is in the vicinity of about 20 dB, this can result in a significant error in the measurement of Q of the resonator. To demonstrate this, we measured the L-band resonator Q with a trombone (line-stretcher) phase shifter in the line between the circulator and the resonator, adjusted to "critical" coupling as judged by a Smith chart display, and then changed the phase and repeated the Q measurement. By selecting positions on the Smith chart that gave maximal undercoupling and maximal overcoupling due only to changes of about 1/8 wavelength in the length of the transmission line, we measured Q changes of about $\pm 13\%$, in accordance with standard transmission line theory.

Since the errors are believed to be random and uncorrelated, the probable error is the square root of the sum of the squares of the probable errors of the individual measurements, where the probable errors are multiplied by the exponent of the factor to which they relate in Eq. [1]. The significant sources of uncertainty are bridge gain (15%), modulation amplitude (5%), square root of power (20%), and Q (13%). The uncertainty in

one signal measurement is then

$$MeasError = \sqrt{0.15^2 + 0.05^2 + 0.2^2 + 0.13^2} = 29\%. \quad [18]$$

For ratios of signal measurements, the total error would be multiplied by $\sqrt{2}$, for a total comparison error of 41%. This error is not unrealistic in view of the number of parameters involved. It is not significant in view of the fact that the difference in the expected ratios of signal strength was a factor of 6.

RESULTS

The results of the measurements on the 3 samples for 7 comparisons (14 total measurements) are given in Table 6. The parameters for these measurements are also given. The last column gives the normalized signal ratio. In each case the signal was normalized to the higher frequency measurement, so the ratio for the higher frequency is always unity. For a 6-fold reduction in frequency our prediction is that the signal at the lower frequency increases by a factor of 1.57. This means that the signal will be 6 times that predicted by Poole at the lower frequency. Table 6 shows that the average of the VHF to L-Band measurements gave a factor of 1.52, which is nearly that predicted. The agreement of predicted and measured results was not quite as good for the L-Band to X-Band case, yielding a factor of 1.14. However, the results for this case are still more than 4 times the result predicted by Poole (*12*), and our best estimate of the uncertainty in the comparison is 41%, as described above.

The calculated and experimental signal intensity ratios are judged to be in agreement within the experimental uncertainty.

DISCUSSION

The resonator frequencies, Q values, and B_1 values agreed with the values predicted from the construction of the resonator, except that the Q of the small L-band resonator was somewhat larger than predicted. This agreement, together with the variations in the EPR signal amplitude with frequency, confirms the background theory and the predictions of frequency dependence. Note that the experimental results show that for the case studied here the EPR signal intensity is actually greater at lower RF/microwave frequency.

The sample lowers the Q and the frequency more in the large L-band and X-band resonators than in the 250-MHz and small L-band resonators. This is because the capacitive gap is larger relative to the inductive loop diameter in the large L-band and X-band resonators than in the other two resonators. A 25-mm o.d., 19-mm i.d. quartz tube full of water reduced the Q of the 250-MHz resonator from 1170 to 905, and a 4-mm o.d., 3.0-mm i.d. tube full of water reduced the Q of the small L-band resonator from 517 to 366 (517 was measured by the decrement method and is somewhat higher than the value in Table 4). Note that the high filling factors of these resonators result in some

TABLE 6
Comparison of Theoretical to Measured Ratio of EPR Signal Height as a Function of Frequency

Sample	Q	Freq. (GHz)	Linewidth (mT)	Pack. den. (g/cc)	Power (mW)	Mod. (G)	Gain	Signal height	Normalized sig. ratio
Tempone in	1008	0.2494	0.117	1	1	0.5	0.333×10^5	20264	1.63
4 : 1 mineral	489	1.535	0.117	1	0.48	0.496	0.8×10^3	15243	1
oil : toluene	—	—	—	—	—	—	—	—	—
	1745	1.5129	0.113	1	0.8	0.20	0.8×10^3	20141	1.31
	698	9.1246	0.112	1	0.256	0.122	0.32×10^4	14597	1
—	—	—	—	—	—	—	—	—	—
BDPA	1006	0.2493	0.082	1.24	1	0.20	0.1×10^6	20036	1.42
1 : 22936 KCl	496	1.5344	0.080	1.176	0.33	0.20	0.2×10^4	11971	1
	—	—	—	—	—	—	—	—	—
	1006	0.2493	0.082	1.24	1	0.20	0.333×10^5	7046	1.52
	496	1.5344	0.080	1.176	0.33	0.20	0.2×10^4	11971	1
	—	—	—	—	—	—	—	—	—
	2333	1.5062	0.078	1.24	0.8	0.20	0.4×10^3	14439	1.06
	954	9.1265	0.078	1.176	0.022	0.19	0.4×10^4	14337	1
—	—	—	—	—	—	—	—	—	—
Ultramarine blue	1005	0.2493	2.41	1.27	25	2	0.333×10^4	8148	1.33
1 : 100 KCl	497	1.5342	2.04	1.19	3.3	2	0.25×10^3	16560	1
	—	—	—	—	—	—	—	—	—
	1858	1.4993	2.06	1.27	3.4	1.56	0.125×10^3	15903	1.05
	866	9.1280	1.99	1.19	0.256	1.22	0.63×10^3	13077	1

Normalized signal ratio (1 : 6 frequency ratio)

Theory—Poole	Theory—Rinard	Ave. VHF to L-band	Ave. L-band to X-band	Ave. all measurements
0.26	1.57	1.52	1.14	1.33

"unexpected" effects. For example, most EPR spectroscopists familiar with using 4-mm o.d. tubes in an X-band TE_{102} cavity think of toluene as a "lossless" sample. However, such a tube of toluene decreased the Q of the 4.3-mm diameter X-band LGR from 1180 to 380. This loss is probably due to methyl group rotation. In order to minimize the Q effect, the tempone samples were prepared in 9 : 1 mineral oil : toluene. Even with this mixture, the Q decreased 41% for the X-band LGR and 42% for the large L-band LGR but only 5% for the small L-band LGR. This large change in Q at X-band could be a factor in the larger error between X- and L-band measurements than that for the L-band to VHF measurements.

Finally, note that this paper reports only EPR signal amplitudes, not signal-to-noise (S/N), because the resonator and spectrometer systems have not yet been optimized for lowest noise. We verified that when a 50-Ω load was put on the input of the 250-MHz bridge in place of the resonator, the measured noise at the output of the bridge was that expected for the thermal noise of the 50-Ω load plus the contributions from the gains and noise figures of the components in the bridge. The noise in the 250-MHz CW EPR spectra appears to be RF source-noise limited.

CONCLUSIONS

When both the resonator size and the sample size are scaled with the inverse of RF/microwave frequency, ω, the intensity of unsaturated, linear-response, CW EPR signal at constant B_1 scales as $\omega^{-1/4}$. The measurements reported here constitute a rigorous confirmation for CW EPR of the theory presented in our recent papers, just as Refs. (*10, 11*) confirmed the theory for pulsed EPR.

ACKNOWLEDGMENTS

This research was supported by NIH Grants GM57577 (GAR) and GM21156 (GRE). The construction of the magnet and bridge was supported by NSF Grant DMI-9523205 to Omni Engineering and the University of Denver.

REFERENCES

1. G. R. Eaton and S. S. Eaton, The future of EPR instrumentation, *Spectroscopy* **3,** 34–36 (1988).
2. G. R. Eaton and S. S. Eaton, Workshop on the future of EPR (ESR) instrumentation—Denver, Colorado, August 7, 1987, *Bull. Magn. Reson.* **10,** 3–21 (1988).
3. S. S. Eaton and G. R. Eaton, The future of electron paramagnetic resonance spectroscopy, *Spectroscopy* **8,** 20–27 (1993).
4. S. S. Eaton and G. R. Eaton, The future of electron paramagnetic resonance spectroscopy, *Bull. Magn. Reson.* **16,** 149–192 (1995).
5. H. J. Halpern and M. K. Bowman, *in* "EPR Imaging and in Vivo EPR" (G. R. Eaton, S. S. Eaton, and K. Ohno, Eds.), pp. 45–63, CRC Press, Boca Raton, FL (1991).
6. T. F. Prisner, Pulsed high frequency/high-field EPR, *Adv. Magn. Opt. Reson.* **20,** 245–299 (1997).
7. G. R. Eaton, S. S. Eaton, and G. A. Rinard, Frequency dependence of EPR sensitivity, *in* "Spatially Resolved Magnetic Resonance: Methods, Materials, Medicine, Biology, Rheology, Geology, Ecology, Hardware" (P. Blümler, B. Blümich, R. Botto, and E. Fukushima, Eds.), pp. 65–74, Wiley-VCH, Weinham (1998).
8. G. A. Rinard, S. S. Eaton, G. R. Eaton, C. P. Poole, Jr., and H. A. Farach, Sensitivity, *in* "Handbook of Electron Spin Resonance" (C. P. Poole, Jr. and H. A. Farach, Eds.), Vol. 2, pp. 1–23, Amer. Inst. of Phys., New York (1999).
9. G. A. Rinard, R. W. Quine, S. S. Eaton, and G. R. Eaton, Frequency dependence of EPR sensitivity, *in* "Biological Magnetic Resonance" (L. J. Berliner, Ed.), in press.
10. G. A. Rinard, R. W. Quine, R. Song, G. R. Eaton, and S. S. Eaton, Absolute EPR spin echo and noise intensities, *J. Magn. Reson.* **140,** 69–83 (1999).
11. G. A. Rinard, R. W. Quine, J. R. Harbridge, R. Song, G. R. Eaton, and S. S. Eaton, Frequency dependence of EPR signal-to-noise, *J. Magn. Reson.* **140,** 218–227 (1999).
12. C. P. Poole, Jr., "Electron Spin Resonance: A Comprehensive Treatise on Experimental Techniques," pp. 394–420, Wiley–Interscience, New York (1967).
13. G. A. Rinard, R. W. Quine, S. S. Eaton, and G. R. Eaton, Frequency dependence of EPR signal intensity, 248 MHz to 1.4 GHz, *J. Magn. Reson.* **154,** 80–84 (2002).
14. J. S. Hyde, *in* "Electron Spin Resonance: Techniques and Applications," p. 200, Wiley–Interscience, New York (1968).
15. R. W. Quine, G. A. Rinard, B. T. Ghim, S. S. Eaton, and G. R. Eaton, A 1-2 GHz pulsed and continuous wave electron paramagnetic resonance spectrometer, *Rev. Sci. Instrum.* **67,** 2514–2527 (1996).
16. G. A. Rinard, R. W. Quine, S. S. Eaton, and G. R. Eaton, Microwave coupling structures for spectroscopy, *J. Magn. Reson.* **105,** 137–144 (1993).
17. W. H. Perman, M. A. Bernstein, and J. C. Sandstrom, A method for correctly setting the rf flip angle, *Magn. Reson. Med.* **9,** 16–24 (1989).
18. S. S. Eaton, G. R. Eaton, J. W. Stoner, R. W. Quine, G. A. Rinard, A. I. Smirnov, R. T. Weber, J. Krzystek, L.-C. Brunel, and A. Demortier, Multifrequency EPR of ultramarine blue, *Appl. Magn. Reson.* **21,** 563–570 (2001).
19. J. H. Van Vleck, The dipolar broadening of magnetic resonance lines in crystals, *Phys. Rev.* **74,** 1168–1183 (1948).
20. E. L. Ginzton, "Microwave Measurements," p. 448, McGraw–Hill, New York (1957).
21. H. H. S. Javadi, Microwave materials, *in* "Handbook of Microwave Technology," Vol. 2, pp. 605–643, Academic Press, San Diego (1995).
22. R. S. Alger, "Electron Spin Resonance: Techniques and Applications," p. 153, Wiley–Interscience, New York (1968).
23. "Tables of Dielectric Materials," Vol. IV, Laboratory for Insulation Research, MIT (1953).